Vibration Energy Harvesting IC Design with Incorporation of Two Maximum Power Point Tracking Methods

Jiayu Li

Thesis submitted to the faculty of the Virginia Polytechnic Institute and State University in partial fulfillment of the requirements for the degree of

Master of Science
In
Electrical Engineering

Dong S. Ha
Daniel M. Sable
Yang Yi

May 11, 2020
Blacksburg, Virginia

Keywords: vibration energy harvesting, dual-input dual-output switching converter, maximum power point tracking

Vibration Energy Harvesting IC Design with Incorporation of Two Maximum Power Point Tracking Methods

Jiayu Li

ABSTRACT

The proposed vibration energy harvesting IC harvests energy from a piezoelectric transducer (PZT) to provide power for a wireless sensor node (WSN). With a traditional rectification stage, a two-path three-switch dual-input dual-output architecture is adopted to extract power and regulate the output voltage for the load with one stage. The power stage is controlled with a new maximum power point tracking (MPPT) algorithm, which integrates both fraction open circuit voltage (FOCV) and perturb and observe (P&O). The proposed algorithm was able to extract maximum power from a transducer due to high accuracy on the maxim power point (MPP) and low power dissipation.

The proposed circuit is implemented in TSMC 180 nm BCD technology and the post-layout simulation verifies the functionality of the proposed design. The simulation results show that the circuit operates under the maximum power point to extract maximum power from a PZT.

Vibration Energy Harvesting IC Design with Incorporation of Two Maximum Power Point Tracking Methods

Jiayu Li

GENERAL AUDIENCE ABSTRACT

The battery life has always been problematic ever since electronic devices exist. As semiconductor technology advances, more transistors could fit in the same area. Resultantly, portable, and mobile devices become more powerful but usually dissipate more power. Unfortunately, the development of the batteries has not been improved significantly. So, it is necessary to charge portable and mobile devices often or replace batteries frequently. In some applications where a device is hard to reach once installed, charging or replacing the battery is difficult. Under these circumstances, energy harvesting from ambient sources is an effective alternative.

There are many types of sources of energy widely available in the environment such as vibration, thermal, solar, RF and etc. Solar energy harvesting is the most popular owing to high power density. However, sunlight is unavailable during night time. Vibration energy, although the power density is lower compared with solar, is a viable solution when solar is not a good source of energy.

The proposed work utilizes abundant vibration energy at factories to power wireless sensor nodes (WSNs), which can monitor the temperature, light intensity, pressure, etc.

Acknowledgements

My sincerely thanks to Dr. Dong S. Ha, for being my advisor ever since undergraduate study. Thanks Dr. Ha for his patience when I know nothing as an undergraduate, his guidance throughout the graduate study, and his leadership for the Multifunctional Integrated Circuits and Systems (MICS) group. Dr. Ha leads the group as a place that mixes hard work and fun. It has been a great journey. I would also like to thank Dr. Dan Sable and Dr. Yang Yi for serving as my committee members. Thanks for taking time and effort to help me on my graduate study.

I am extremely appreciative of Dr. Dan Sable and the Bradley Department of Electrical and Computer Engineering for providing the teaching assistantships throughout my graduate study. I learnt not only the technical knowledge, but also interpersonal skills as a teaching assistant.

I would like to thanks my peers in the MICS group: Junjie Wang, Alante Dancy, Long Huang, Fairbirz Lohrabi Pour, Jinhua Wang, Ryan Reed, Xinye Liu, Keyvan Ramezanpour, Shenghou Ma, Kangjun Bai, Shiya Liu, Hongyu An, Yibin Liang, Qiyuan An, Chenyuan Zhao, Victor Gan , Fabiha Nowshin, Kevin Tomkins, Jiayuan Zhang, Moqi Zhang, Shinwoong Park. Thank you for all the help you have given to me. It was a great pleasure working with you.

Lastly, I would like to thank my parents, Peifen Li and Junwei Li, and sister Ziyu Li. I could not have been able to accomplish this far without their love, support, and understanding.

Table of Contents

List of Figures

List of Tables

Chapter 1: Introduction

1.1 Motivation

In many applications, the demand for self-powered devices has increased for the past decades, such as wireless sensor nodes (WSNs), biomedical implants, wearable devices, etc. Harvesting energy from ambient seems to be a viable solution to power those electronic devices. Energy harvesting lowers the maintenance of battery such as charging or replacing [1]-[7]. A typical WSN only needs μW during sleep mode, but around mW during transmission mode. As shown in Figure 1.1, there are mainly four sources of energy from ambient environments with the different power density and power ranges. Among the four, solar energy has the highest power density, hence the highest power rating. Vibration energy has a relatively lower power density than solar; it can harvest power ranges from μW to mW which is sufficient to power a WSN. Piezoelectric energy transducer (PZT) is one type of transducer that harvests the vibration energy and convert to electrical energy.

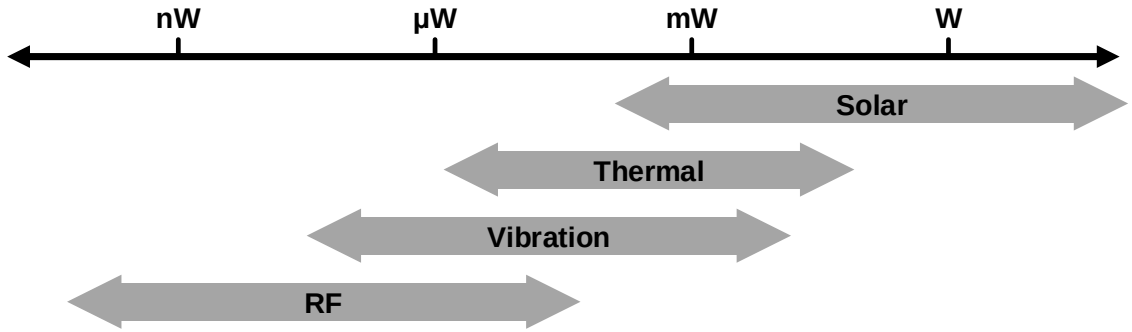

Figure 1.1 Power range of energy sources

1.2 Proposed Work and Technical Contribution

In this work, an energy harvesting IC design targets for vibration energy harvesting from factories to power the wire sensor node. The power conditioning circuit is carefully designed based on the source characteristics and output requirement. To serve a wider range of input and load condition, the dual-input and dual-output architecture with constant on time pulse skipping modulation is adopted. The major contribution of this work is the new maximum power point tracking method proposed. It utilized two existing commonly practice maximum power point tracking methods, adopts the advantages, and compensate for the disadvantages of one method by the other one.

The proposed IC design was built in Cadence virtuoso environment with TSMC 180 nm BCD technologies. A custom layout for the IC is also built-in Cadence, the post-layout simulation results indicate the correct functionality that was designed.

1.3 Organization of this Thesis

The remainder of this thesis is organized as follows. Chapter 2 provides background information on the transducer used for vibration energy harvesting. Followed by the existing power conditioning circuit. Then, two current existing MPPT methods are discussed with their own advantages and disadvantages. Chapter 3 presents the proposed IC design in detail by first introducing the dual-input dual-output architecture adopted for the power stage along with the control scheme. Second, the proposed MPPT method is demonstrated with the flowchart and waveforms. Chapter 4 presents the layout of the IC and the post-layout simulation results of this design. Finally, Chapter 5 will draw the

conclusions, the proposed improvement could be done in the future work that could possibly increase the efficiency and reliability of the energy harvesting system.

Chapter 2: Preliminaries

This chapter provides background information on vibration energy harvesting. In Section 2.1, the type of transducer used for the vibration energy harvesting system is introduced along with its modeling and characteristics. The basic operation of the dual-path three-switches converter is presented in Section 2.2. In section 2.3, two maximum power point tracking methods are discussed.

2.1 Piezoelectric Transducer

There are two types of transducers that are most common for vibration energy harvesting, the piezoelectric transducer (PZT) and the electromagnetic generator (EMG). The PZT usually generate high voltage but low current output, while the EMG usually generate low voltage but high current output. In this study, the PZT is used to convert vibration energy into electrical energy.

2.1.1 PZT Modeling

The PZT generates electrical energy by stressing the piezoelectric material via vibration. Fig. 2.1 presents the equivalent electromechanical model of PZT that is widely adopted in the research and Table I summarizes all the parameters used in the model [8]-[9].

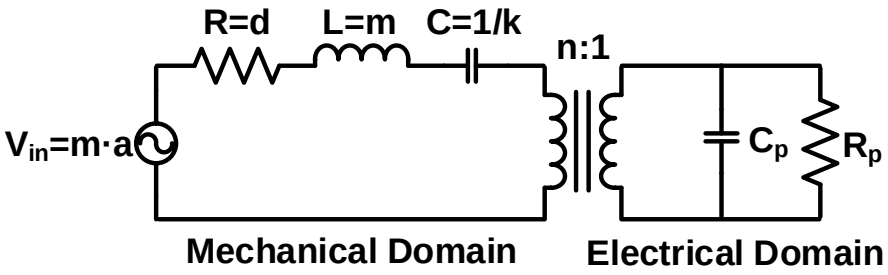

Figure 2.1 Equivalent electromechanical model

Table 2.1 Electromechanical model parameter

Symbol	Parameters
m	Vibrating mass
a	Clamping velocity
d	Viscous damping coefficient
k	Spring constant (stiffness)
n	Electromechanical coupling coefficient
Cp	Parasitic capacitance
Rp	Parasitic resistance

As an external exciting force is applied to a PZT by its own vibrating mass and clamping acceleration, a sinusoidal exciting velocity, Vin, with the vibration frequency, f, is then converted into electrical domain by a coupling coefficient, n. Since the parasitic resistance is magnitudes higher than the equivalent impedance of parasitic capacitance as $R_p \gg 1/(2\pi f C_p)$, Rp could be ignored. Therefore, this model could be simplified to Fig. 2.2.

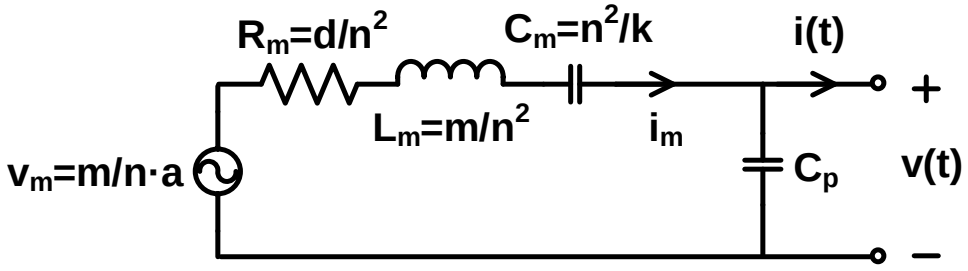

Figure 2.2 Simplified PZT model

2.1.2 PZT Characteristics

One unique characteristic of PZT is that unlike the resistive impedance of the PV cells and TEGs, the nature of the impedance to the PZT is capacitive and is highly dependent on the operation frequency. The equivalent internal impedance, Zs, from Figure 2.2. is

$$Z_s = \left(\frac{d}{n^2} + \frac{j2\pi fm}{n^2} + \frac{k}{j2\pi fn^2}\right) // \frac{1}{j2\pi fC_p} \tag{1}$$

Equation (1) can be rewritten into the form of $Z_s = R_s + jX_s$, where

$$R_s = \frac{n^2 d}{(2\pi f)dC_p + \left(n^2 + kC_p - (2\pi f)^2 mC_p\right)^2}$$

$$X_s = \frac{(2\pi f)^2\left(n^2 m - d^2 C_p\right) - ((2\pi f)^2 m - k)^2 C_p - n^2 k}{(2\pi f)^2 dC_p + (2\pi f)\left(n^2 + kC_p - (2\pi f)^2 mC_p\right)^2}$$

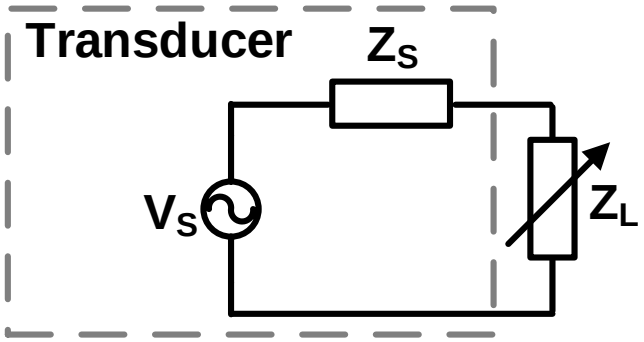

Figure 2.3 Maximum power extraction

To achieve maximum power extraction at the load for a source with complex internal impedance as shown in Figure 2.3, complete impedance matching is desired. Under this condition, the load impedance is $Z_L = Z_s^* = R_s - jX_s$, and the output power is

$$P_L = \frac{1}{2}\left|\frac{V_s}{Z_s + Z_L}\right|^2 R_s = \frac{1}{2}\left|\frac{V_s}{2R_s}\right|^2 R_s = \frac{|V_s|^2}{8R_s} \tag{2}$$

However, it is not practical to match complex impedance in application as the circuit complexity is higher. Considering for pure resistive load, the load impedance should be $Z_L = |Z_s| = \sqrt{R_s^2 + X_s^2}$, and the output power is

$$P_L = \frac{1}{2}\left|\frac{V_s}{Z_s + \sqrt{R_s^2 + X_s^2}}\right|^2 R_s \tag{3}$$

In real application where a PZT is tested in [10], The electromechanical parameters extracted from this PZT is presented in Table II. As seen in Figure 2.4 where the impedance over a range of frequency is plot, the impedance of a PZT is highly depend on the operation frequency. In addition, the impedance is purely resistive at the resonance frequency of the PZT. Hence, peak power extraction for pure resistive load matching exists at resonance frequency as shown in Figure 2.5.

Table 2.2 Electromechanical parameters used in simulation

Symbol	Parameters	Value
m	Vibrating mass	0.1286
d	Viscous damping coefficient	15.5067
k	Spring constant (stiffness)	82461
n	Electromechanical coupling coefficient	-0.0196
Cp	Parasitic capacitance	41.24e-9

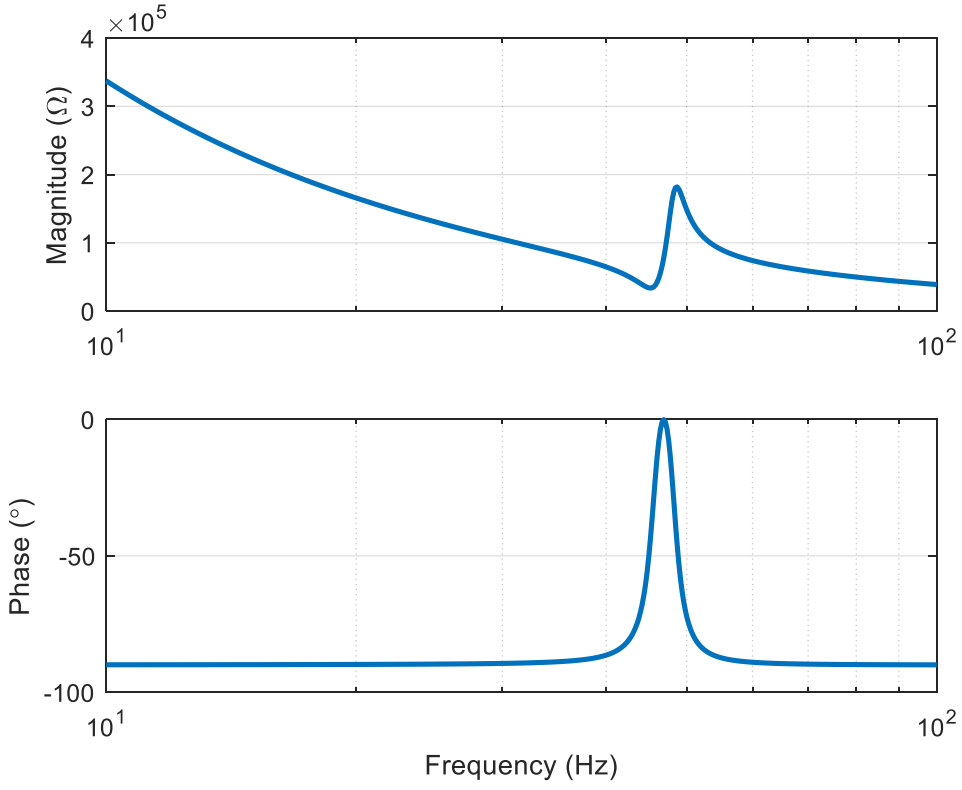

Figure 2.4 Impedance of a PZT

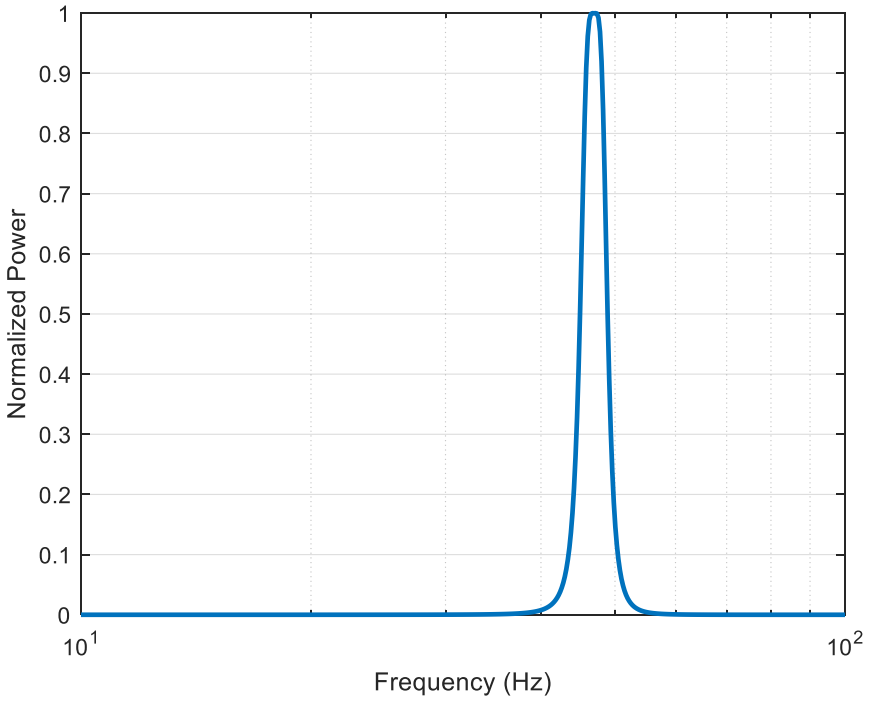

Figure 2.5 Power extraction of pure resistive load

2.2 Power Condition Circuit

In real case scenario, the working environment for the transducer and the load conditions do not stay the same. The piezoelectric transducer generates an AC source and the WSN load required a regulated DC input. A power condition circuit is required to transfer the energy out from the transducer and provides correct DC rail to the load.

2.2.1 Conventional Power Condition Circuit for PZT EH

Conventionally, energy harvesting for PZT usually need an AC to DC converter to convert the AC output of PZT to DC, one DC to DC converter that incorporate a maximum power point tracking (MPPT) interface to extract maximum power, and another DC to DC converter to regulate the output voltage to the load as shown in Figure 2.6. The energy transferred out from the transducer must travel through three stages of

power converters. An extra DC to DC converter stage increases the power loss, hence the two-stage DC to DC converter decrease the energy harvesting efficiency. [7]

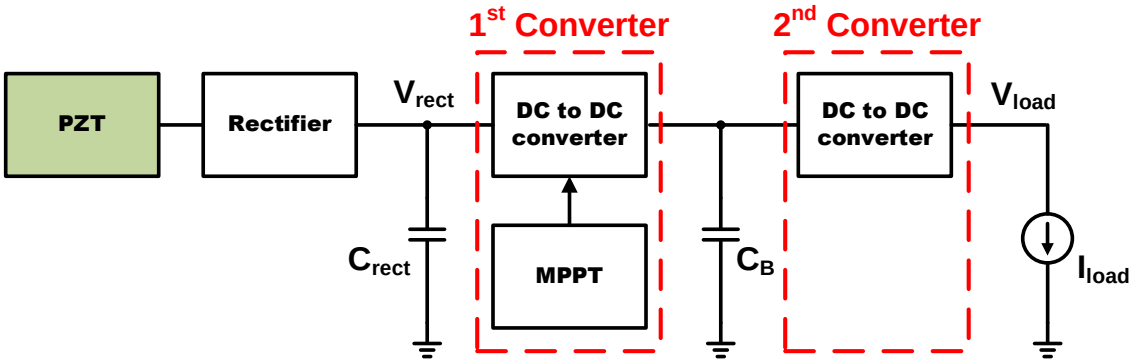

Figure 2.6 Conventional power conditioning circuit for PZT

2.2.2 Dual-Input Dual-Output (DIDO) Converter

Utilizing a battery as both the input and the output element, the traditional two-stage DC to DC converter for maximum power extraction and regulation was able to cut down into one and decrease the lossy elements that energy must travel through to the load. This topology is often called dual-input dual-output (DIDO) converter and has been widely adopted in [11]-[13]. Figure 2.7 demonstrate the system diagram if the PZT energy harvesting adopted the DIDO converter. The energy has a direct path right after the rectification to the load instead of traveling through two stages and could support a smoother load transient and a higher load condition.

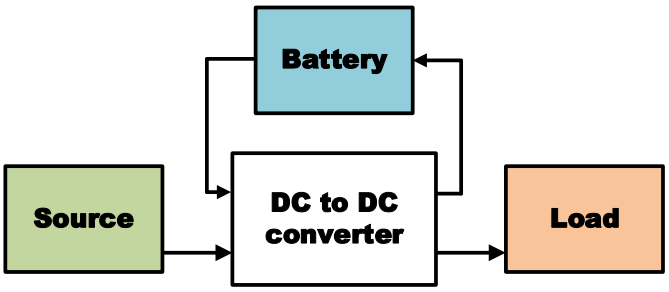

Figure 2.7 Power conditioning circuit with DIDO power converter

2.2.3 Dual-Paths Three-Switches (2P3S) Converter

Different dual-input dual-output structures are deeply discussed with switch loss and inductor size selection, and a two-path three-switches with the highest efficiency is proposed in [12]. The two-path three-switch architecture is shown in Figure 2.8 with three modes of operations detailed in Table 2.3. The first mode is the harvest mode in which the energy was harvested by the buck converter from the source directly to the load by enabling the SW1 as high side switch and SW3 as low side switch. The second mode is the supplement mode where the battery is the input and the load is the output. In this mode of operation, the buck converter is consisting of SW2 as the high side switch and SW3 as the low side switch. The last mode is the charge mode where the excess energy is transferred from the load to the backup battery by a boost converter in which the SW3 is the on switch and SW2 is the off switch. Note that, in order to have the charge mode, the harvest mode must operate first following immediately with the recycle mode.

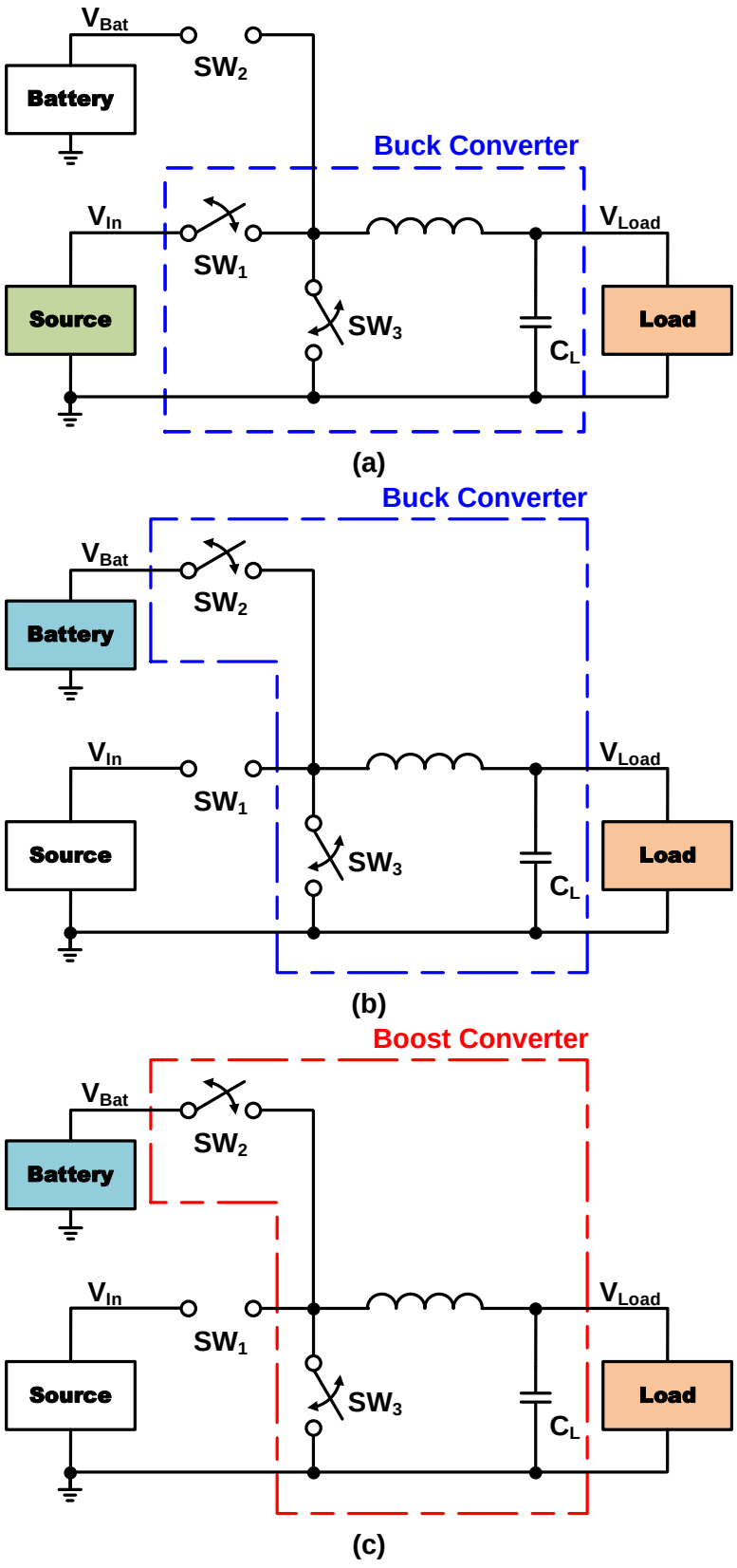

Figure 2.8 2P3S modes of operation (a) harvest, (b) supplement, (c) charge

Table 2.3 2P3S mode of operations

Mode	Ports		Switches			Converter
	Input	Output	SW1	SW2	SW3	
Harvest	Source	Load	Switch	Open	Switch	Buck
Supplement	Battery	Load	Open	Switch	Switch	Buck
Charge	Load	Battery	Open	Switch	Switch	Boost

2.3 Maximum Power Point Tracking Methods

The maximum power point tracking methods allows to monitor the changes in the system and adaptively operate the transducer under maximum power point. Two commonly used MPPT methods are fractional open circuit voltage and perturb and observe, each with its unique advantages and disadvantages.

2.3.1 Fractional Open Circuit Voltage (FOCV)

The fractional open circuit voltage takes samples of open circuit voltage periodically, monitors, and regulates the voltage at the source compared to a fraction of the sampled open circuit voltage [8], [12]-[15]. In the case of PZT energy harvesting, the sampled and monitored open circuit voltage would be the rectified voltage. The control circuit for this algorithm is simple meaning the power consumption is low. A typical sampling circuit is shown in Figure 2.8. The DC to DC converter connecting between the source and the load is disconnected when the sampling clock is high. The open circuit

voltage information is stored in the $C_{S/H}$. The sampling time is typically longer than expected because it needs to wait until the Vrect climb back to the open circuit voltage and charged up the sampling capacitor. This period of disconnection results in loss of energy.

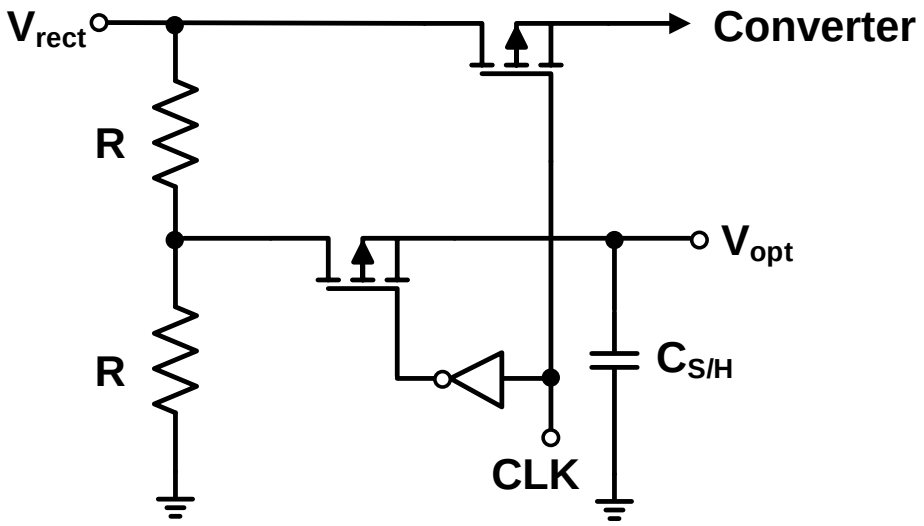

Figure 2.9 Typical sampling circuit for FOCV

The FOCV method utilized a basic circuit theorem that the optimal output voltage is half of the open circuit voltage when the resistive load is not connect to the resistive source.

$$V_{MPP} = k \cdot V_{oc} = \frac{1}{2} V_{OC} \tag{4}$$

However, in the real situation, the optimal operating voltage is not always equal to half of the open circuit voltage. Balato et al. first investigated the closed form of MPP voltage in terms of Voc in [8].

$$V_{MPP} = \frac{I_{SC} V_{OC}}{V_{OC} B_m + \sqrt{B_m^2 V_{OC}^2 - 3(B_m V_{OC} I_{SC} - I_{SC}^2)}} = k \cdot V_{oc} \tag{5}$$

where $B_m = 2\pi f C_p + g$. As seen from equation (5), the fraction is depending on the vibration frequency and the electromagnetic coupling. For weak electromagnetic coupling, the fraction is usually lower show in Figure 2.9 with real data used in [8]. Therefore, the accuracy is highly dependent on the preset value of fraction. If the working environment changes from time to time but the fraction is preset to one value, this MPPT method cannot guarantee the PZT is operating under optimal voltage.

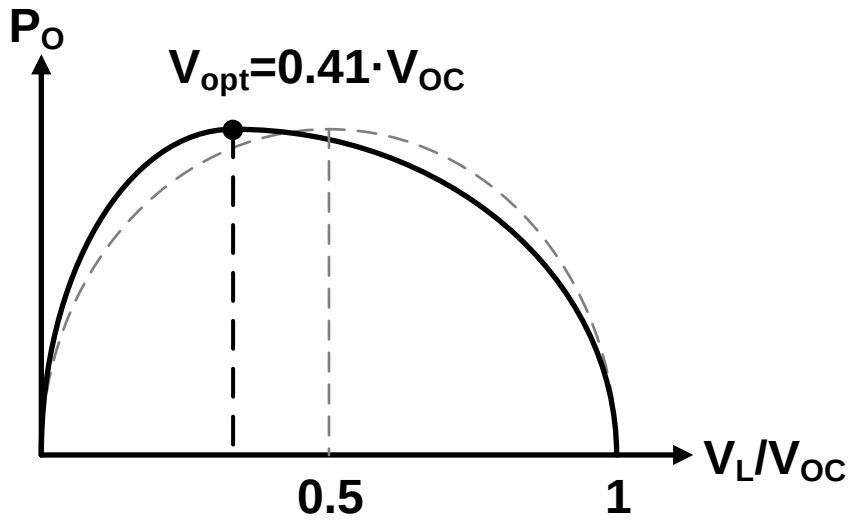

Figure 2.10 Optimal operating voltage for PZT

2.3.2 Perturb & Observe (P&O)

The perturb and observe algorithm monitors the input power changes as one parameter of system changes and make changes to the perturbing parameter direction accordingly [8]-[9], [11], [16]-[17]. Typically, the perturbation parameter is the duty cycle of the power converter, changing the duty cycle of the switching converter consequently change the operating voltage of the source. Once the perturbing parameter changes, the input power is then computed and recorded. Then, two consecutive input power will be compared. If the later input power is higher than the previous one, the

perturbation direction remains the same, vice versa. This algorithm often started from the lowest the power and climb its way up to the highest power available as shown in Figure 2.10; that is why it is also called hill climbing.

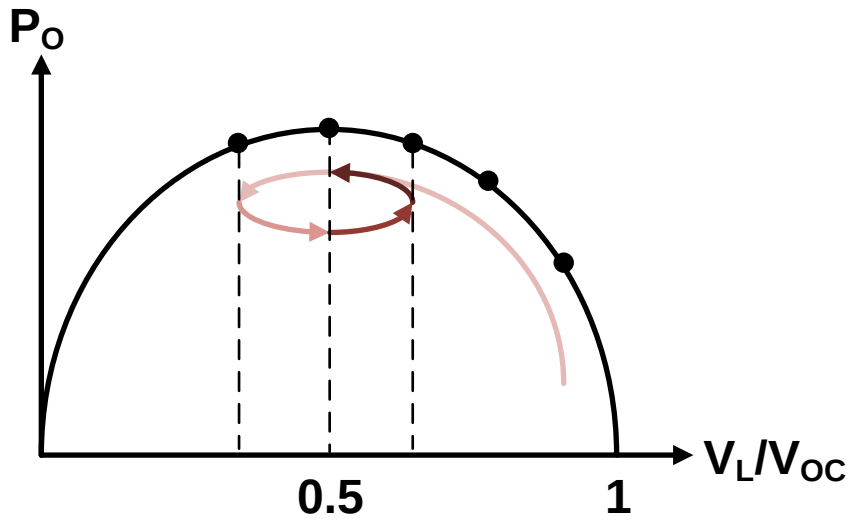

Figure 2.11 P&O visualization

To compare power, a power measurement circuit is required, which is often a power-hungry circuit. Typically, a power measurement circuit consists of a voltage sensor, voltage sensor, and a multiplier. All those building blocks consume a large amount of power which is not suitable for a low power energy harvesting circuit.

A power measurement topology for power converter in an energy-efficient way was proposed in [11] where the length of off-time, t_{off}, in one cycle is directly related to the input power if the output of the converter is regulated.

$$t_{off} = \frac{1}{V_L} \cdot \sqrt{\frac{2 \cdot L \cdot P_{IN}}{f_s}} \tag{6}$$

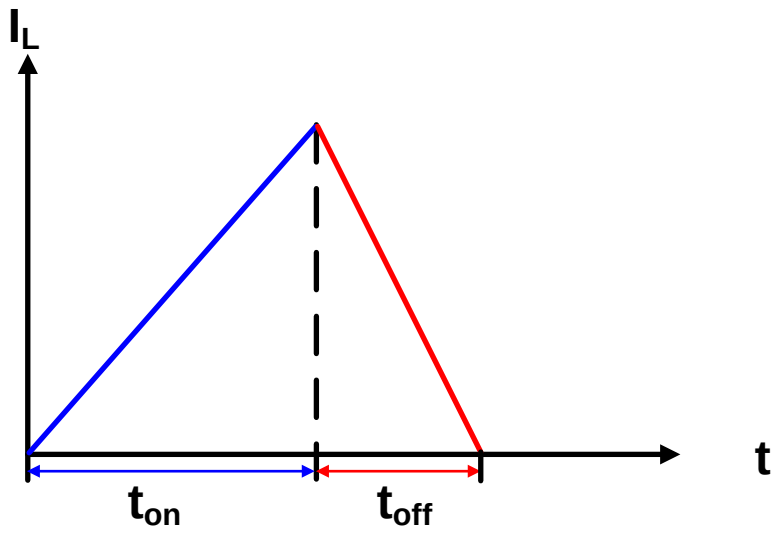

Figure 2.12 Sensor-less power monitor

Based on equation (6), the pulse width of the off time, t_{off}, can represent the input power if the output is regulated, and the switching frequency is fixed. The input power can be represented by counting the number of pulses under a clock that is faster than the system clock for one off time. The input power of a converter is computed without use of sensor, ADC, and multipliers; this is an efficient power measurement solution for the regulated converter.

For the case of variable frequency modulation, the relationship in equation (6) is no longer valid. One single off-time cannot accurately represent the input power. Junjie el al. proposed sampling multiple off-time in a fixed sampling period to solve this issue [17]. The new relationship of off time and input power is described in equation (7).

$$\sum_{0}^{N} t_{off} = \frac{1}{V_L} \cdot \sqrt{\frac{2 \cdot L \cdot P_{IN}}{f_{sample}}} \tag{7}$$

By counting number of off-time along with each off-time's pulse width in a fixed sampling period, it can accurately represent the input power if the output is regulated.

2.4 Chapter Summary

In this chapter, previous work that is related to the PZT energy harvesting system is discussed. The study of modeling and characteristics for PZT is an important step to determine what type of power conditioning circuit would be the best fit for the system. The dual-input dual-output architecture cut down stages in between the source and the load, thus a better efficiency. Each maximum power point tracking method has its own advantages and disadvantages. A new MPPT method that adopts the advantages and compensates for the disadvantages of two MPPT methods mentioned will be proposed in the next chapter.

Chapter 3: Proposed EH IC Design

In this chapter, the proposed energy harvesting IC design for a PZT will be detailed described. In Section 3.1, the two-path three-switch converter is adopted as the main power stage that achieved maximum power extraction and regulation for the load at the same time. Section 3.2 proposed a new maximum power point tracking method that incorporates two commonly adopted methods mention in the last chapter. To make a complete energy harvesting system, the start-up capability will be discussed along with some basic building blocks in ICs.

3.1 Power Stage Design

The input of the system is a high voltage low current AC source from PZT. The AC to DC rectification will not be the focus of this design. A full-bridge rectifier or a negative voltage converter with a lower loss on active rectification can convert the AC input to a DC output, V_{rect}. To extract maximum power after rectification stage and regulate the load voltage, a dual-input dual-output converter is desired due to its lower power consumption and higher flexibility of load conditions as compared to traditional two stages of DC to DC converters. Hence, as shown in Figure 3.1, the power stage is composed of a rectifier and a dual-input dual-output converter in which the dual-path three-switches converter [12] is adopted.

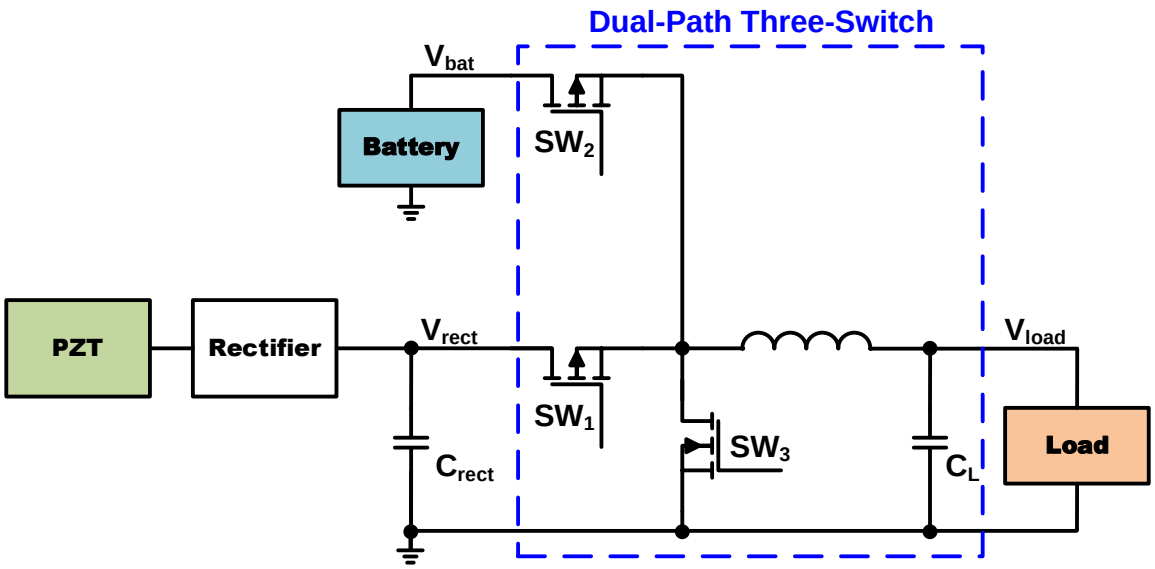

Figure 3.1 Proposed power stage

3.1.1 Two-Paths Three-Switches (2P3S) Converter

Generally, the rectified voltage, V_{rect}, is considered as a high voltage (greater than 5 V) as compared to the primary load, typically a WSN that is regulated at 1.8 V. A buck converter is desired to converter high voltage from rectified PZT source to low voltage for load. If the light load condition exits, the PZT may produce excess energy than the load required. The excess energy could be store in a secondary storage element like a coin cell battery. The stored energy could be reused once the input cannot produce sufficient energy to the load. Adding one more switch on top of the basic buck converter structure enables the secondary storage element as both an input and an output port depending on the mode of operations. Therefore, the two-paths three-switches (2P3S) converter is adopted as the main power converter for the system. As mentioned in the previous chapter, there are three modes of operations for 2P3S converter. To easily control the operations of converter, a 2-bit signal is assigned to represent each mode of

operation as shown in Table 3.1. The uses of this selection bit will be further discussed in section 3.1.2 and 3.1.3.

Table 3.1 2P3S mode selection bit

Mode	Selection bit	
	S1	S0
Harvest	0	0
Supplement	0	1
Recycle	1	0

3.1.2 Constant On-time Pulse Skipping Modulation (COT-PSM)

There are multiple modulation schemes available for power converters. The converter can operate in fixed frequency modulation or variable frequency modulation. The variable frequency can provide a wider range of load operations, it is a better option if light load condition is expected. [12] The variable frequency control scheme adopted for this two-path three-switches is constant on-time pulse skipping modulation. Under a fixed frequency system clock, the inputs and outputs are compared with the references in each cycle and determine whether the pulse should be skipped or not. For example, if V_{load} is low and V_{rect} has sufficient energy to supply, the pulse will not be skipped as EN goes high, and the on-time generator will generate an on pulse to transfer energy out from PZT to the load. In the case where V_{load} and V_{bat} are sufficiently high, the pulse would be skipped until the next clock pulse. The on-time and off-time generation is shown in

Figure 3.2. The on-pulse is precisely controlled by a bias current and a timing capacitor. The off-time generation is enabled after a falling edge detector of the on-pulse. It monitors the off switches' voltage to detect zero current. Since different switches are used in different modes of operations, the 2-bit mode selection bit is used to determine which is the on-switch and which is the off-switch. With the use of multiplexer and demultiplexer along with the mode selection bit, only one on-time block and one off-time block is needed.

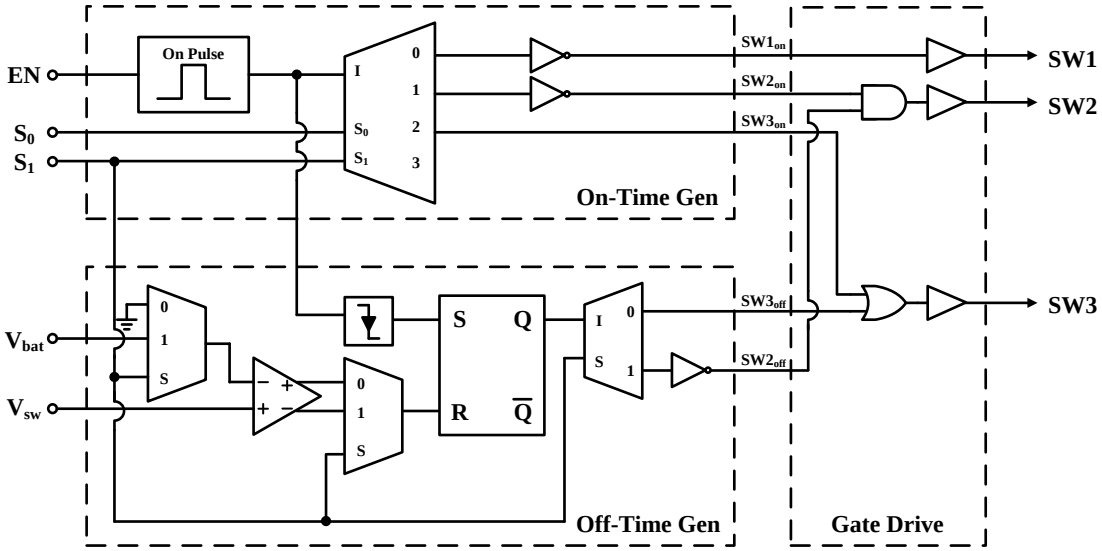

Figure 3.2 On-time & off-time generation

3.1.3 I/O Monitor & Mode Selection

To determine the mode selection bit, the rectified PZT input (V_{rect}), the load (V_{load}), and battery (V_{bat}) are monitored by three clocked comparators under system clock and generated three corresponding signals as shown in Figure 3.3. The rectified input would be compared with sampled open circuit voltage which will be further discussed in the next section. The load and the battery are compared with internal references such that load is regulated to 1.8 V and the battery is regulated to 3.7 V respectively.

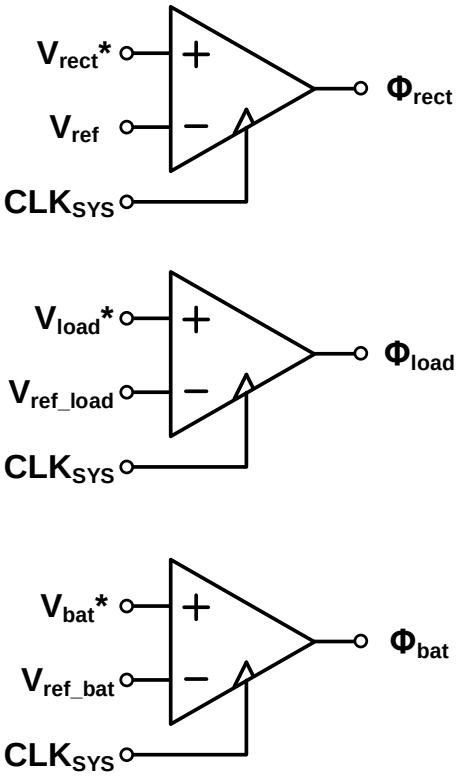

Figure 3.3 I/O monitoring circuits

Table 3.2 I/O monitoring & mode selection logic

Φ_{rect}	Φ_{load}	Φ_{bat}	Mode	Selection bit	
				S1	S0
L	L	L	Deactivated	x	x
L	L	H	Supplement	0	1
L	H	X	Deactivated	x	x
H	L	X	Harvest	0	0
H	H	L	Charge	1	0
H	H	H	Deactivated	x	x

The 2-bit mode selection bit that represents modes of operations is the logic combinations of the outputs of three comparators as shown in Table 3.2. These two-bit signals are then sent to an on-time & off-time generation block shown previously.

3.2 Proposed MPPT Method

In the previous chapter, two maximum power point tracking method has been illustrated with both their own advantages and disadvantages. In this section, a new MPPT method is proposed. It adopts the advantages of one method and compensate for the disadvantages of the other one.

3.2.1 Method Overview

The advantages and disadvantages of two previously discussed MPPT methods are shown in Table 3.3. The proposed MPPT method incorporates these two commonly used MPPT methods to gets an accurate MPP in an energy efficient way. However, the control circuit is complex which means more die area and the energy harvesting is interrupted under a fixed frequency.

Table 3.3 MPPT methods comparison

MPPT	FOCV	P&O	Proposed
Advantages	Simple control Energy efficient	Accurate MPP	Energy efficient Accurate MPP
Disadvantages	Inaccurate MPP Interrupted harvesting	Complex control Power hungry Long convergence	Complex control Interrupted harvesting

3.2.2 Method Flowchart and Waveforms

Figure 3.4 is the flowchart of the proposed MPPT method, and Figure 3.5 is the expected waveforms for rectified voltage. The proposed MPPT methods will start from FOCV mode, and it stores two consecutive open circuit voltage, Voc(n) and Voc(n-1). The FOCV mode is running under a fixed frequency, and it takes a sample of open circuit voltage at the beginning of each cycle. After sampling the open circuit voltage of the rectified voltage, V_{rect}, and hold it at Voc(n). At the end of the sampling period, there is a parameter, V_{th}, is computed and compared with a preset value, Δ.

$$V_{th} = |Voc(n) - Voc(n-1)| \tag{8}$$

Equation 8 shows that the V_{th} is the absolute difference of two consecutive open circuit voltage samples. If the V_{th} is higher than Δ, then the P&O block will get triggered and start perturbing and looking for MPP. Before it enters P&O mode, the V_{rect} will first converge to half of open circuit voltage. Hence, the fraction, k, which is the perturbation parameter started from half in P&O mode. The P&O mode stops once MPP is found and locked k at optimal, k_{opt}. On the other hand, if the V_{th} is lower than the preset values, then P&O mode will not get triggered, the FOCV mode will continue to regulate the Vrect at the fraction, k, of open circuit voltage (or the optimal voltage found from the previous cycle) until the next cycle of FOCV mode.

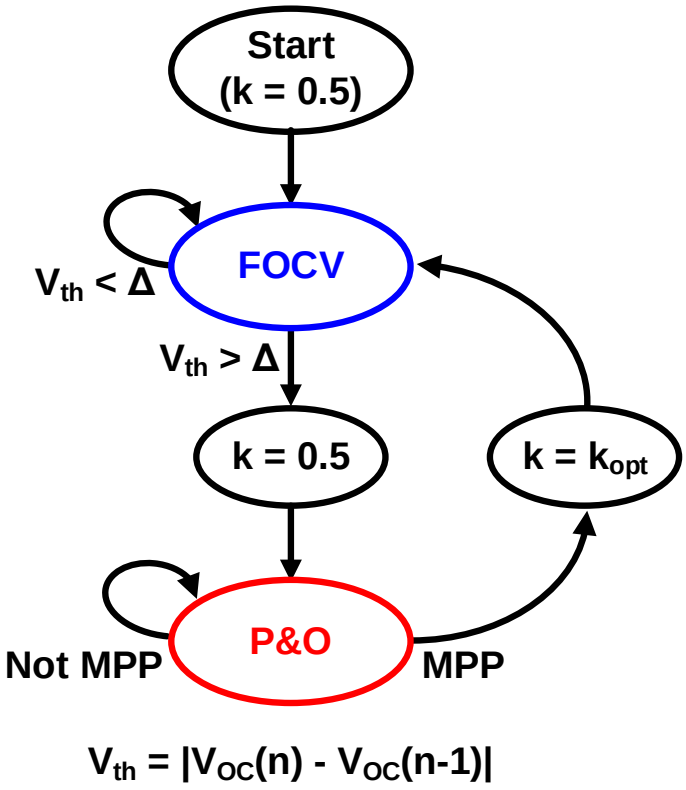

Figure 3.4 Proposed MPPT method's flowchart

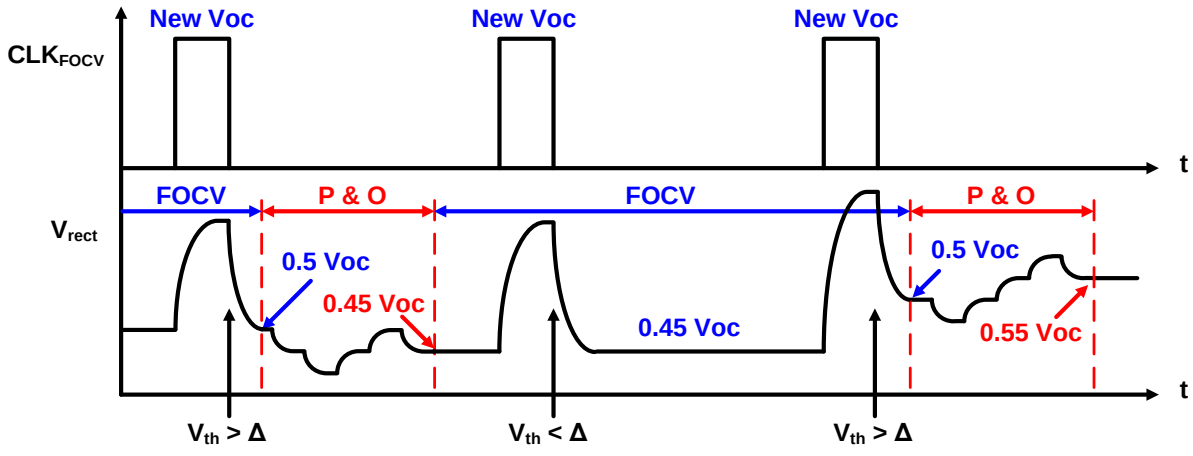

Figure 3.5 Proposed MPPT method's expected waveforms

3.2.3 FOCV mode

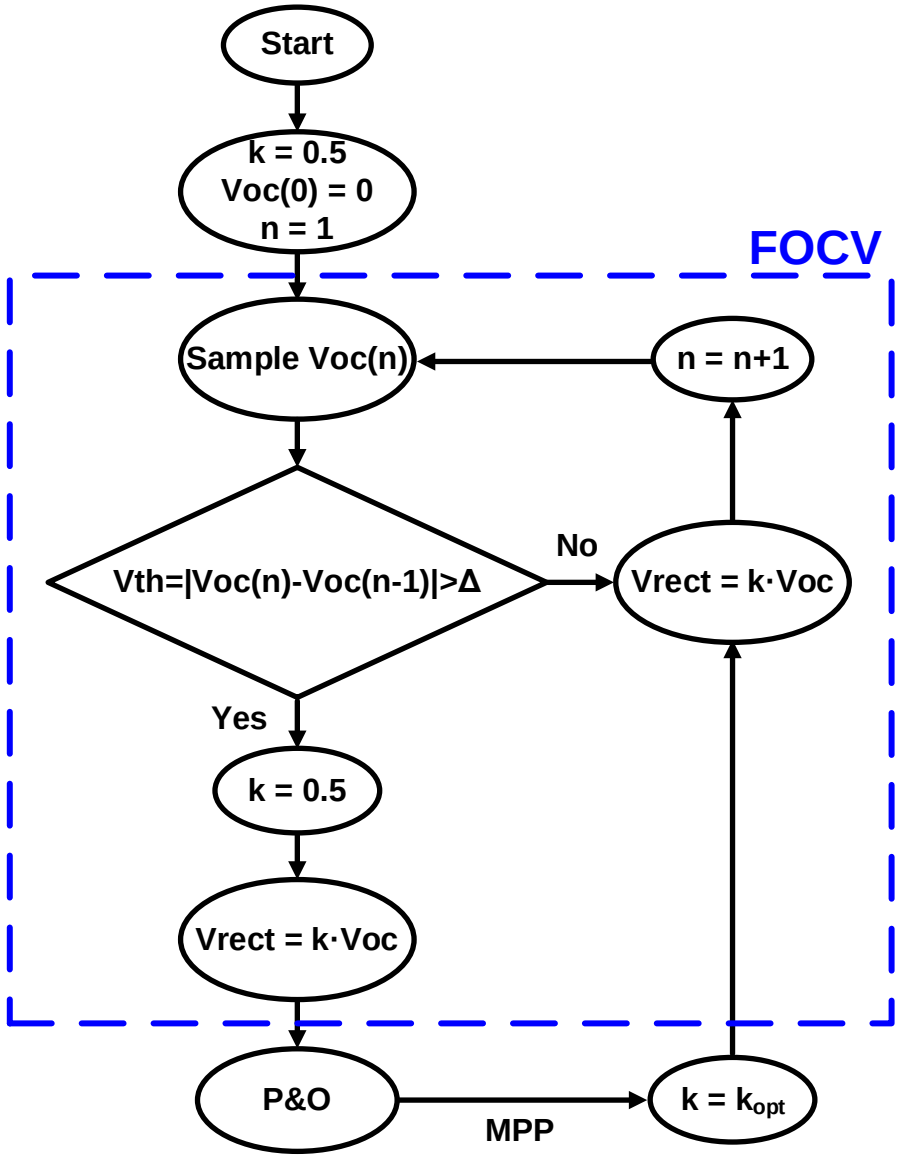

Figure 3.6 FOCV flowchart

The flowchart with further details on FOCV mode is shown in Figure 3.6. The FOCV block operates under a FOCV clock with a fixed frequency of 0.1Hz and 30ms of on pulse. Figure 3.7 demonstrates the circuit used to sample the open circuit voltage. Once the FOCV clock becomes high, the SW1 will no longer get switched disconnecting the load from the source ($V_{rect} = V_{oc}$).

During the sample period, the battery will continue to supply energy to the load if the load needs it and the battery have sufficient energy. SW4 in Figure 3.7 will then connect Vrect to a sample capacitor and charged up the open circuit voltage of Vrect. The sample cap is chosen such that it can hold the open circuit voltage of Vrect until the next sample period comes in, therefore, the sampling time required to charge up the capacitor is long, which in this case is 30ms.

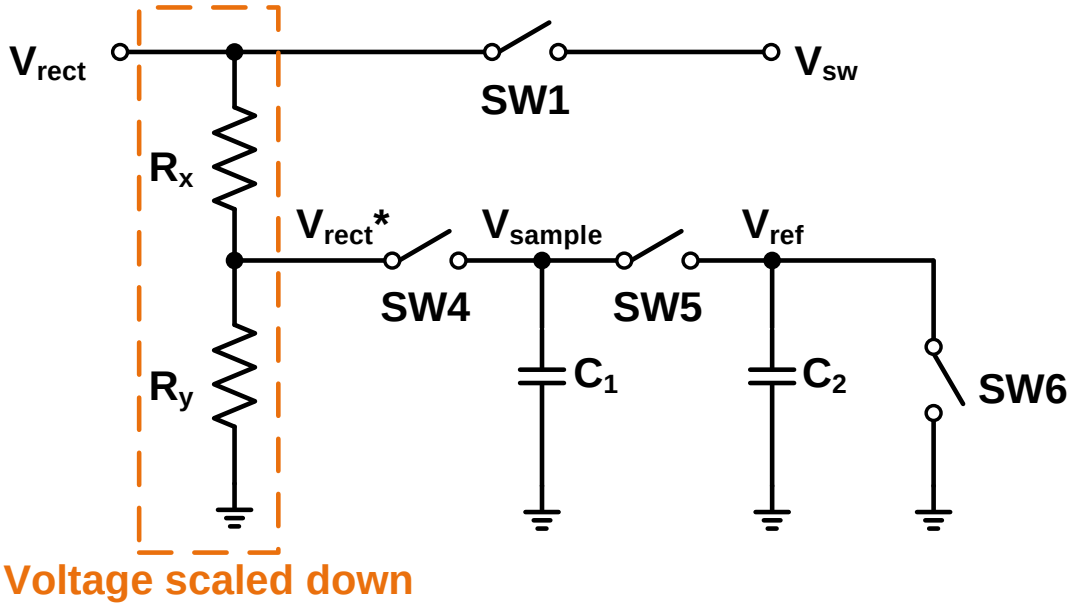

Figure 3.7 FOCV sampling circuit

Note that the resistors here are not used to get to half of open circuit voltage, but to scale down the open circuit voltage as shown in equation 9.

$$V_{rect} *= k \cdot V_{oc}, \qquad k = \frac{R_y}{R_x + R_y} \tag{9}$$

To get half of the sample scaled open circuit voltage, the same size capacitor is used to connect to the sampled voltage. The voltage is half immediately after the SW5 is closed based on the charge sharing theorem for capacitors as shown in equation 10. SW6

is connected when SW4 is connected to discharge any remaining charge on the capacitors. The expected waveform of sampling circuit is shown in Figure 3.8.

$$V_{ref} = V_{sample} = \frac{1}{2} \cdot k \cdot Voc \tag{10}$$

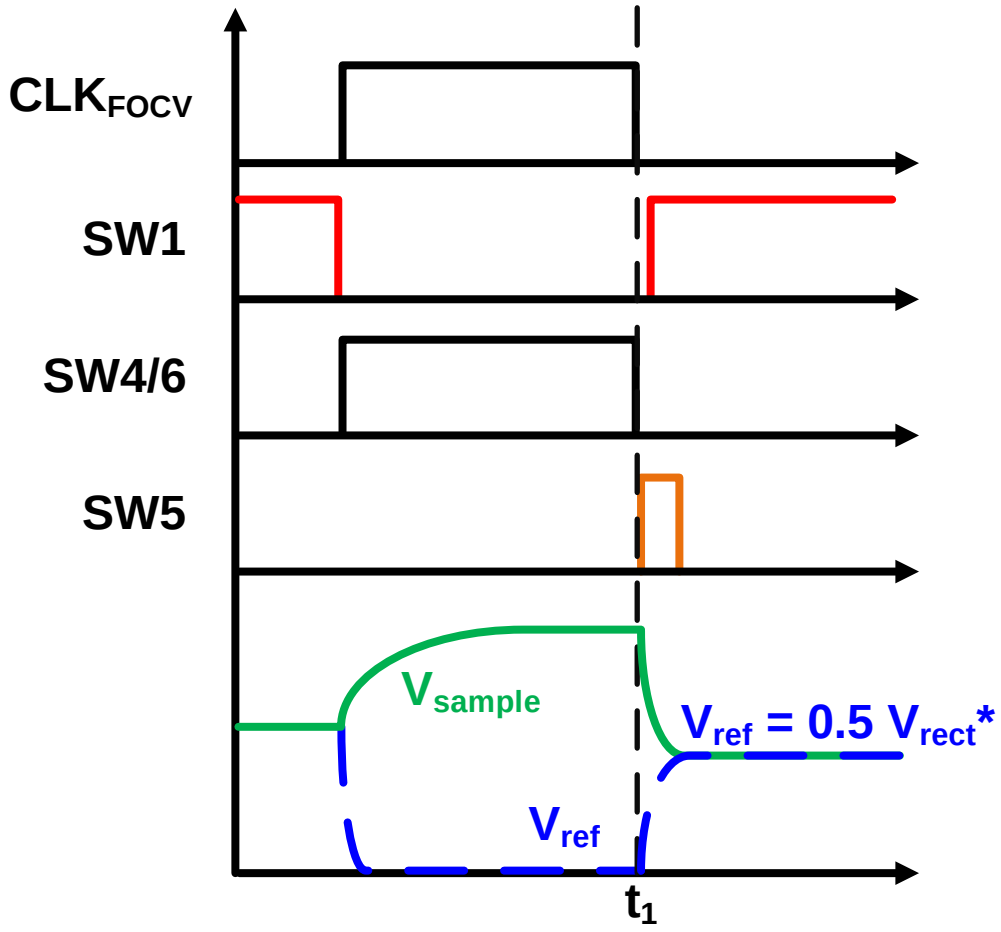

Figure 3.8 FOCV sampling circuit expected waveforms

To compute the V_{th}, same set of sampling circuit in Figure 3.7 is used to obtained two consecutive open circuit voltage and store into different storage capacitors, C_1 and C_3. These two capacitors take turns to store the open circuit voltage information. In addition, two hysteresis comparators are used to determine whether two consecutive sampled voltages have a difference higher than the preset value as shown in Figure 3.9. If

two consecutive samples have an absolute difference that is greater than Δ, then signal Φ1 and Φ2 will be at the opposite logic level, and vice versa. This preset value, Δ, is controlled by the hysteresis of the comparators. With an XOR gate and a D flip-flop, Φ_{trig} will trig high when Φ1 and Φ2 are at the opposite logic level. This signal will be used to reset the P&O block shown in the next section.

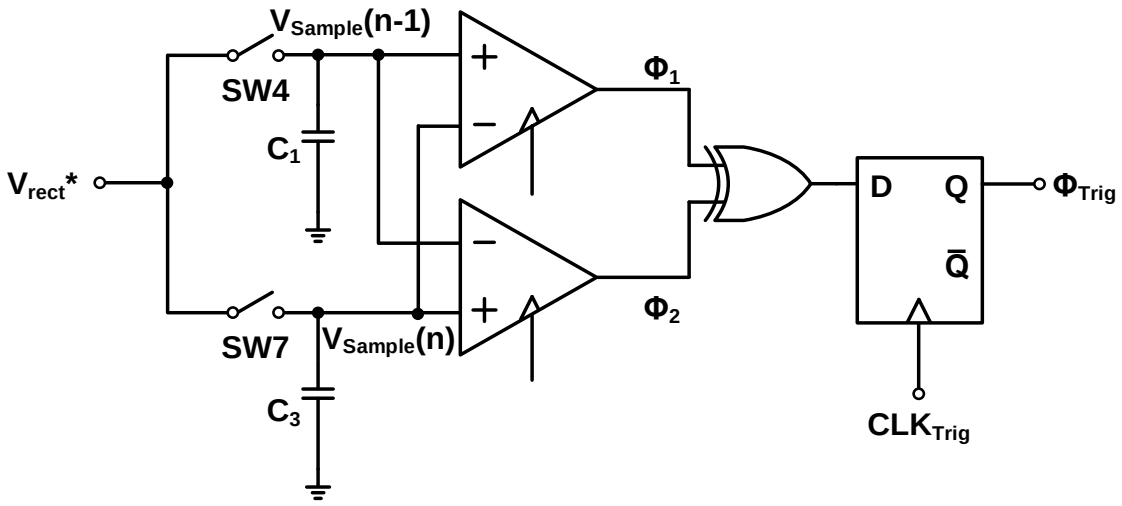

Figure 3.9 FOCV decision circuit

3.2.4 P&O mode

The P&O MPPT method has three key components, perturb a parameter, observe the power change, and decide the next perturbing direction. Unlike solar panels where its maximum power point is at around 80% of its open circuit voltage, the maximum power point for piezoelectric transducer is usually around 50%. Normally P&O method would start from 100% of open circuit voltage and work its way up to find the maximum power point. If this process is used to find the maximum point of PZT, it's a waste of time and energy going from 100% to around 60% when we know that the MPP of PZT is around

50%. Since the open circuit voltage is available from the FOCV mode, the perturbing parameter is set to be the fraction, k, of the open circuit voltage. In this proposed method, the P&O mode will start from 50% of the open circuit voltage of V_{rect} and start perturbing with a smaller perturbation step size. As stated in equation 9 and 10, the sampled open circuit voltage is only a fraction of the rectified voltage. Now, if the fixed resistor Rx in Figure 3.7 is replaced with a resistive ladder controlled by a 3-bit signal, R<2:0>, as shown in Figure 3.10, then the fraction of this rectified voltage could be converted to equation 11.

$$k' = \frac{R_y}{R_x' + R\langle 0\rangle \cdot R_0 + R\langle 1\rangle \cdot R_1 + R\langle 2\rangle \cdot R_2 + R_y}$$

$$V_{rect}{}^{*} = k' \cdot V_{rect} \tag{11}$$

Denote $k_{opt}{}'$ is the optimal fraction in which the transducer is operating under the MPP. The true rectified voltage with respect to open circuit voltage is derived in equation 12.

$$V_{rect}{}^{*} = k_{opt}{}' \cdot V_{rect}$$

$$V_{ref} = \frac{1}{2} k \cdot V_{OC}$$

$$V_{rect}{}^{*} = V_{ref}$$

$$k_{opt}' \cdot V_{rect} = \frac{1}{2} k \cdot V_{OC}$$

$$V_{rect} = \frac{1}{2} \cdot \frac{k}{k_{opt}'} V_{OC}$$

$$V_{rect} = k_{opt} \cdot V_{OC},\ where\ k_{opt} = \frac{1}{2} \cdot \frac{k}{k_{opt}'} \tag{12}$$

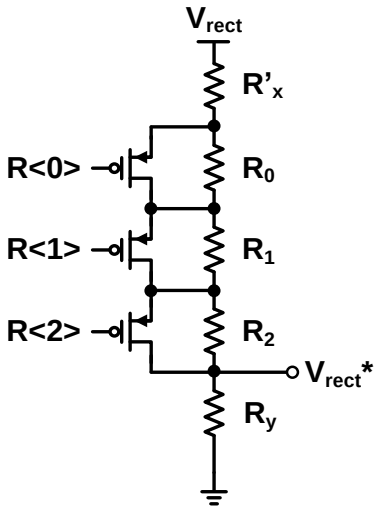

Figure 3.10 P&O perturbation parameter control circuit

To start perturbing at the middle of a sequence, R<2:0> is set to R<2:0>=100 during the sampling period of FOCV and at the beginning of the P&O. An up-down counter is used to control the R<2:0>. A default up-down counter counts up by one bit if the input is high and count down if the input is low; all bit would reset the output to zero during reset. A different version of up-down counter is needed to reset the most significant bit (MSB) of output to high instead of low. The new version of up-down counter is shown in Figure 3.11 where the MSB is connected to the inverted output of JK flip flop.

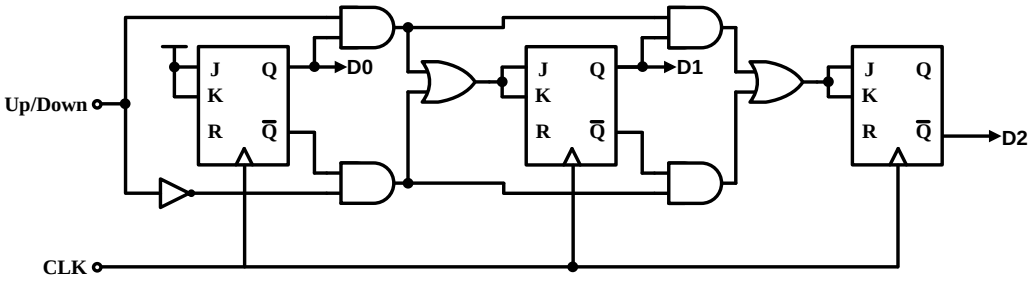

Figure 3.11 New up-down counter

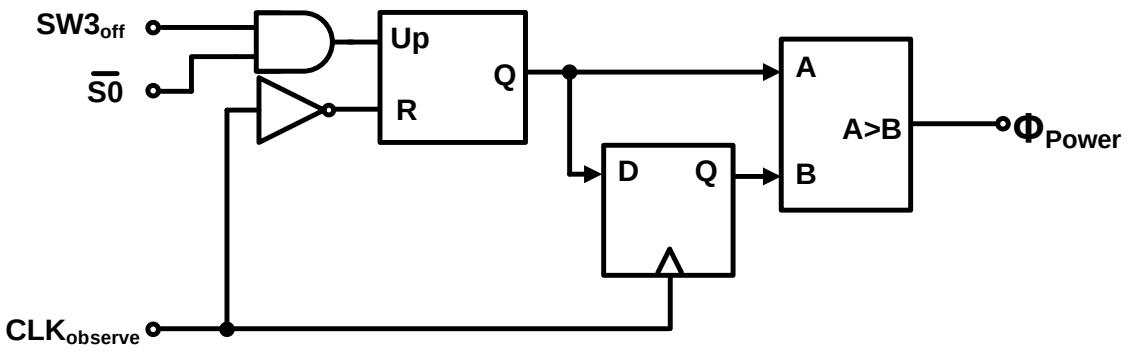

Figure 3.12 P&O power measurement circuit

To observe the power change from perturbation, first a power measurement circuit is needed. As discussed in section 2.3.2, measuring the off-time of a power converter is directly related to the input power. Therefore, comparing the off-time is sufficient to tell the power change of the system. For the proposed system using COT-PSM, the power converter is working under a variable frequency. The new method of measuring multiple off-time in a fix sampling time can address the accuracy of the power measurement for variable frequency in [17]. As shown in Figure 3.12, the power measurement circuit is consisted of an up counter, a D flip-flop to store previous data and a digital comparator. To compute the input power, only the off-time during the "harvest" mode is counted.

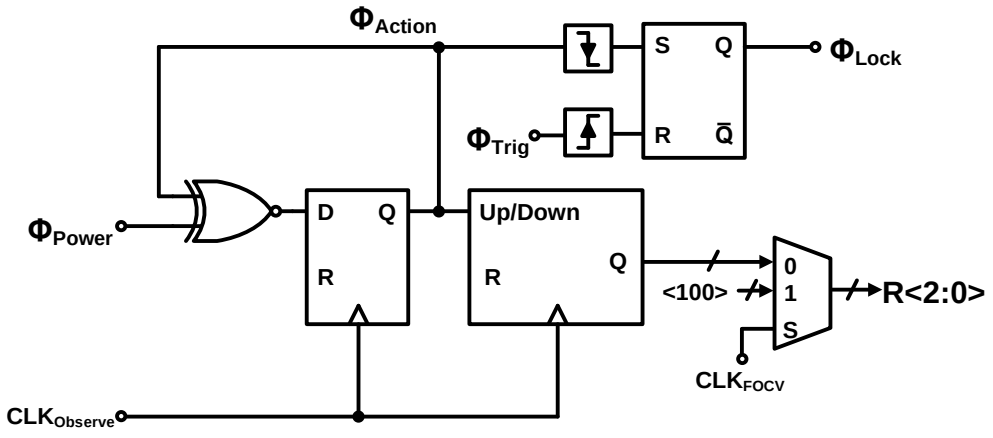

Figure 3.13 P&O decision circuit

Once the power change is obtained, the perturbation direction could be determined. If the input power of current cycle is higher than the previous cycle, the perturbation direction remained the same, and vice versa. The decision circuit for P&O usually consist of a XNOR gate and a D flip-flop as shown in Figure 3.13. The output of the D flip-flop is then sent to a up/down counter that is going to toggle the resistive ladder to get a new reference fraction. In this proposed design, the MPP is found after the perturbation direction changes twice. With a falling edge detector and a SR latch, the signal Φlock indicates the MPP has reached and locked at its MPP until the next P&O is trigger. If the next FOCV mode get triggered without triggering the P&O mode, the FOCV mode will regulate the V_{rect} to the previous found optimal fractional open circuit voltage other than a fixed number 50%. In another situation where P&O get triggered again, the reference bit is reset to R<2:0>=100 and restart the whole process of P&O.

3.3 Bandgap reference & current generation

As seen from the I/O monitoring & mode selection block, it requires internal voltage references to accurately monitor and regulated the inputs and outputs of the converter. Bandgap reference is designed to provide voltage references that are supply independent and temperature independent references. One bandgap reference circuit is shown in Figure 3. 14. The base-emitter voltage, V_{BE}, of a bipolar device is complementary to absolute temperature (CTAT), while the voltage difference between two base-emitter voltages of two bipolar devices is proportional to absolute temperature (PTAT). Adding CTAT to PTAT will cancel out the temperature dependent elements and left with temperature independent voltage [18].

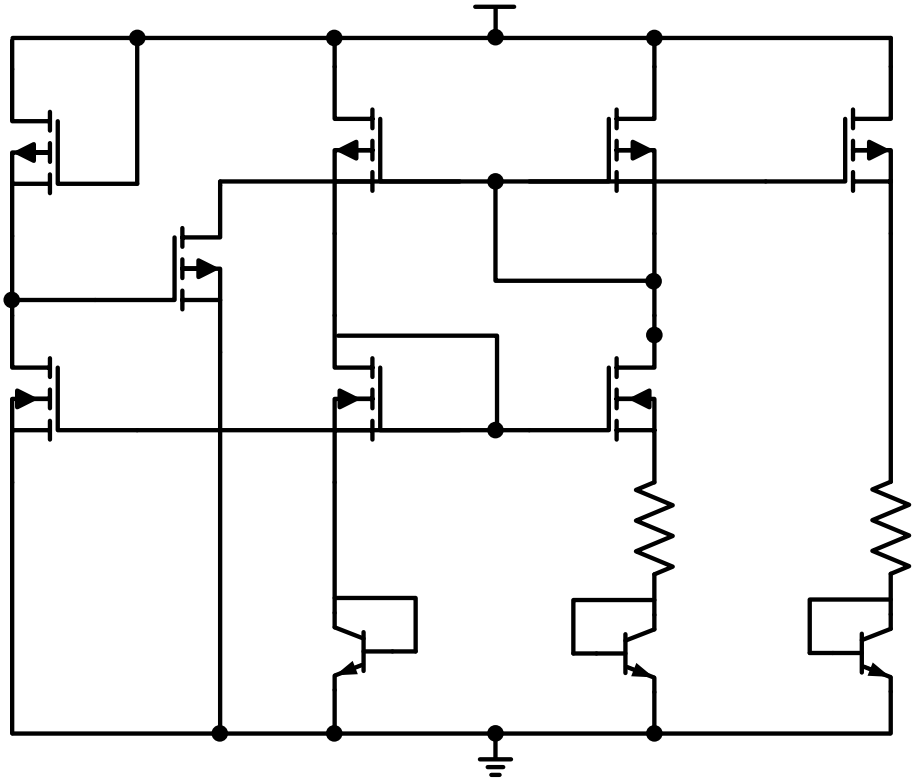

Figure 3.14 Bandgap reference

The bias current is presented in several places of the system. The compared need a bias current to set the correct biasing the differential pair. The on-pulse block in the on-time generation needs a precise bias current to charge a preset cap in order to get an precise on-time. The ring oscillator utilizes the same concept to create clock pulses which also need precise bias current. The current bias circuit should be independent from the supply to provide a precise. As shown in Figure 3.15, the bias current generated is precisely 4 μA and can be replicated with more current mirrors [19].

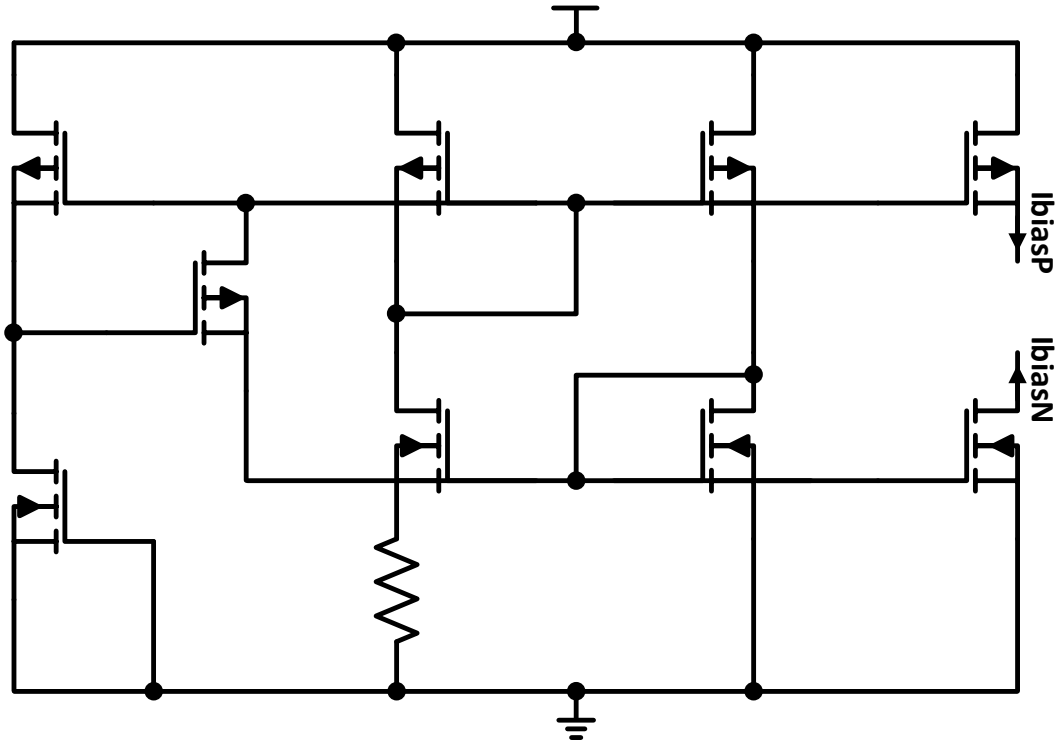

Figure 3.15 Bias current generation

3.4 Chapter Summary

The proposed energy harvesting IC design for PZT is detailed described in this chapter. The two-path three-switch dual-input dual-output converter is adopted with constant on time pulse skipping modulation control scheme. It enables the system with a wider input and output range. The new MPPT method that adapts the advantages of two existing methods and combines them into one is able to operate the transducer under optimal voltage accurately and efficiently.

Chapter 4: System Implementation

In this chapter, the IC design proposed in chapter 3 is implemented using TSMC 180nm BCD technology. System characteristics and the custom layout are shown in section 4.1. The post-layout simulation results demonstrated in section 4.2 verifies the functionality expected in chapter 3.

4.1 System review

4.1.1 system block diagram

Figure 4.1 demonstrates the system block diagram with further details. The system input is the PZT that operate at 500Hz of resonant frequency with a maximum input current of 25 mA, thus the maximum input voltage to the system is around 32 V. The two-path three-switch the converter has inductor and output filter capacitor off-chip and all three power switches are on-chip; all these three power switches has a breakdown voltage of 36V. The switches are controlled by the I/O monitoring & mode selection block which actively monitoring the rectified input to the convert, the 1.8 V load, and the battery voltage. The MPPT block consists of two sub-block, FOCV and P&O, each of them is controlled by the separated clock, CLK_{FOCV} and $CLK_{Observe}$. The three main triggering signals are Φ_{Trig}, Φ_{Lock}. The Φ_{Trig} is generated from the FOCV block to trigger P&O block and Φ_{Lock} is generate from the P&O block to enable the normal operation of FOCV. All the timing capacitors to generate the clock and the resistive ladder are left off-chip for further tuning.

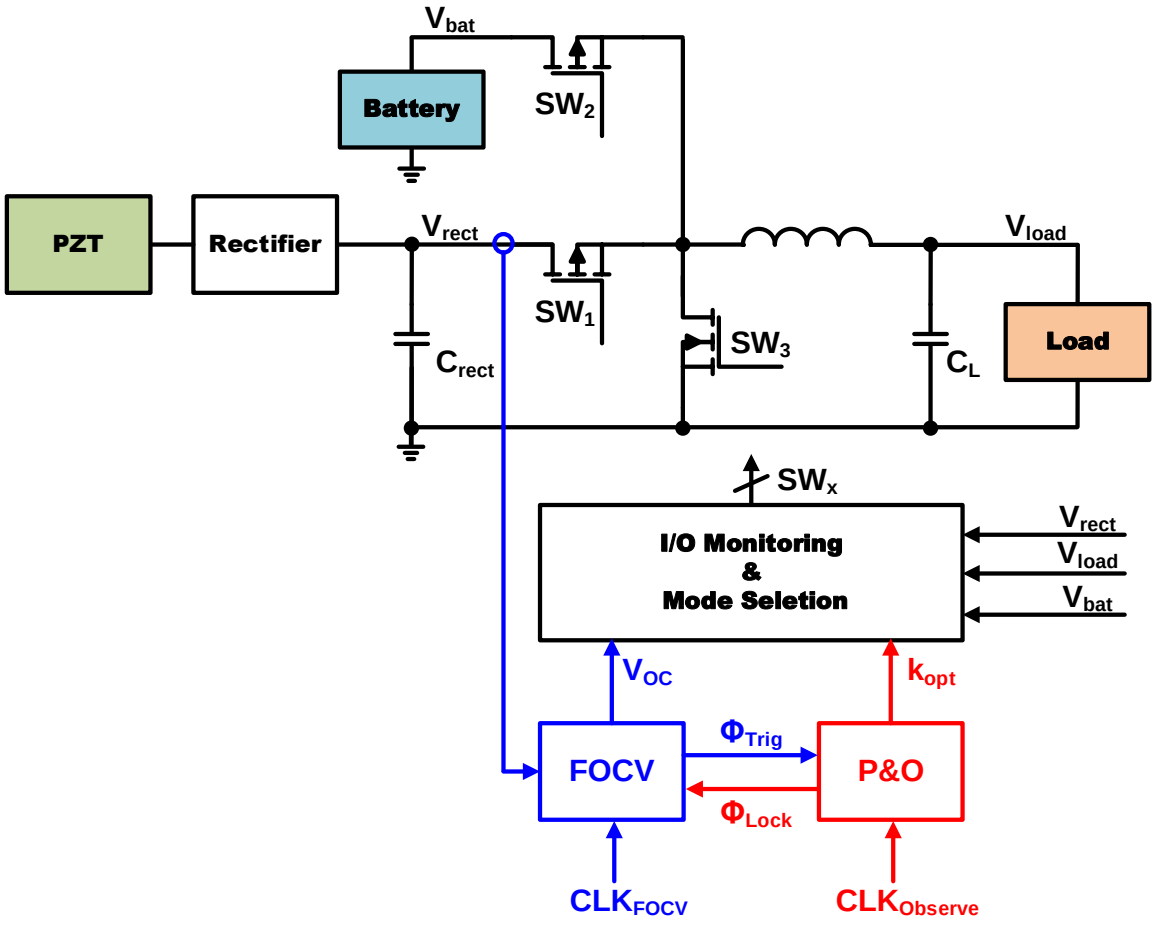

Figure 4.1 System block diagram

4.1.2 Layout

Figure 4.2 shows the custom layout for the proposed IC design. The active die area is around 1mm x 1mm. The majority of the space is occupied by the main switches of the power converter. Since the input voltage is high, the MOSFET for the switch required isolation for protection, hence the size of switch is huge to get a lower on-resistance.

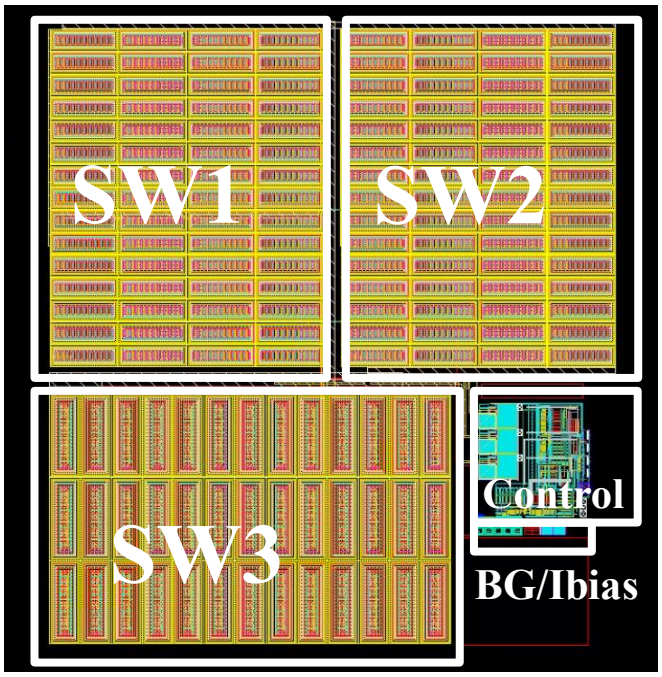

Figure 4.2 Custom layout for proposed IC design

4.2 Post-layout simulation

After the custom layout is generated, post-layout simulation is performed to verifies all the functionalities of each sub-block before tape out.

4.2.1 Power Stage Simulation Results

Figure 4.3 demonstrates the simulation results of the power stage. Constant on-time pulse skipping modulation is achieved by the I/O monitoring & mode selection block where the mode selection bit clearly indicates the mode of each operation. As seen from Figure 4.3, pulses were skipped when load has sufficient voltage. The energy is harvested from PZT when the rectified voltage, V_{rect}, is lower than the reference. The battery provides energy to the load when V_{rect} is lower than the reference. All the ports to 2P3S converter are regulated under constant on-time pulse skipping modulation.

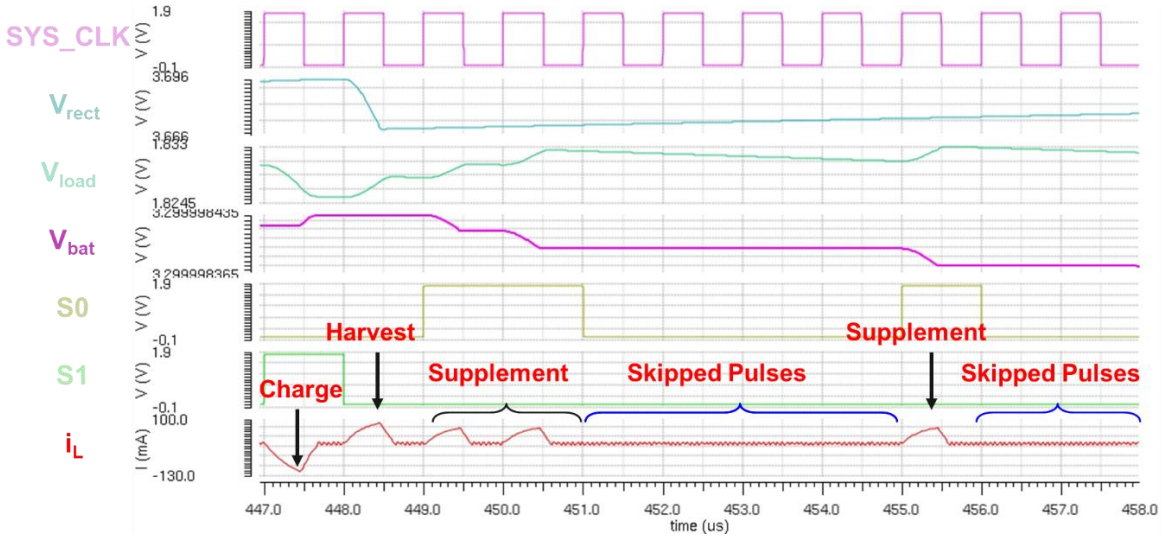

Figure 4.3 Power converter simulation results

4.2.2 MPPT Simulation Results

Figure 4.4 is the simulation results for the FOCV sampling circuit. It clearly shows that the sampling circuit were able to sample the scaled down rectified voltage and trim it by half at the end of sampling period. These waveforms verify the functionality as expected in Figure 3.8.

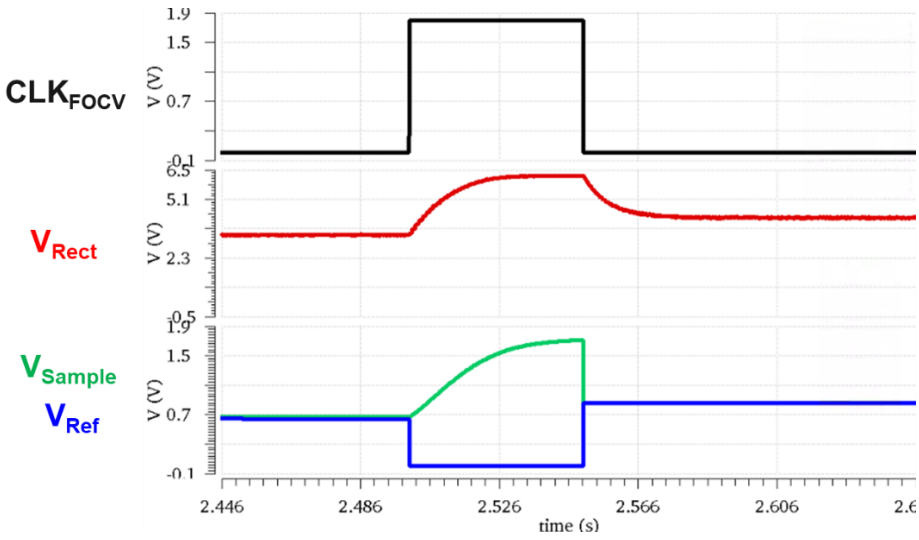

Figure 4.4 FOCV sampling circuits simulation results

Figure 4.5 is the simulation results for the FOCV decision circuit. For the first sampling cycle, since the previous sample was clear to zero at the start, Φ_{Trig} is triggered high as expected. In the second sampling cycle, two samples are the same because the input remains the same, Φ_{Trig} is triggered low as expected. During the third sampling cycle, the input change abruptly, hence two consecutive samples are different and Φ_{Trig} has triggered high again as expected. Therefore, The FOCV decision circuit was able to send out a logic high signal when two consecutive samples are different and a logic low signal when two consecutive samples are the same or fairly close to one another.

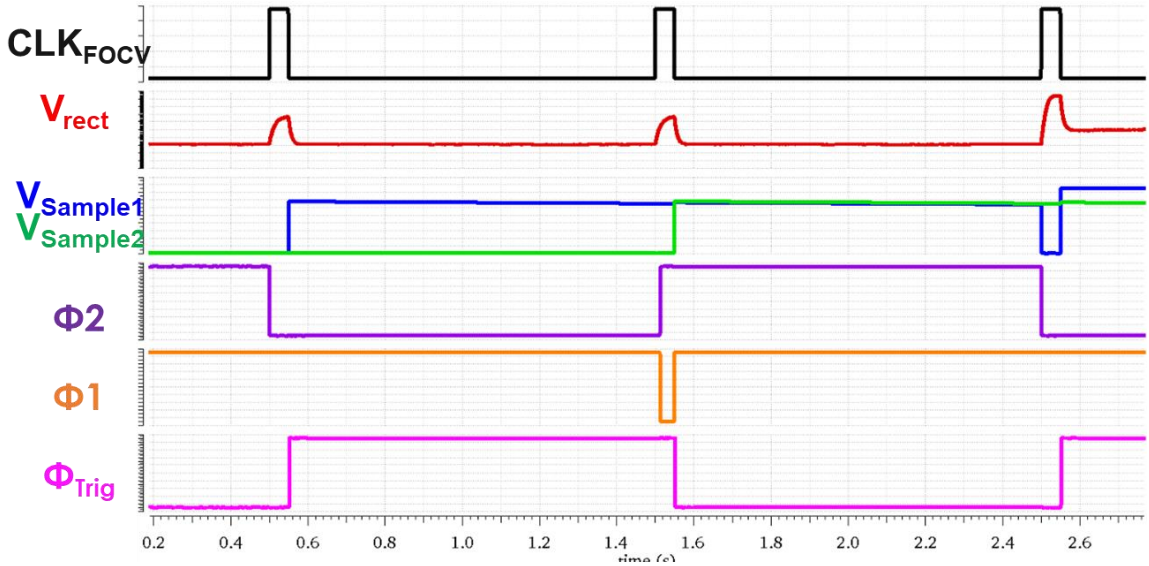

Figure 4.5 FOCV decision circuits simulation results

Figure 4.6 demonstrates the simulation results for the P&O decision circuit. The up-down counter was able to reset the control bit for the resistive ladder R<2:0> to 100. The signal $\Phi_{acition}$ was able to change perturbation direction as power change direction

changes by switching to a different logic level. Φ_{lock} was able to trigger high after the perturbation direction changes twice, hence lock the control bit R<2:0>.

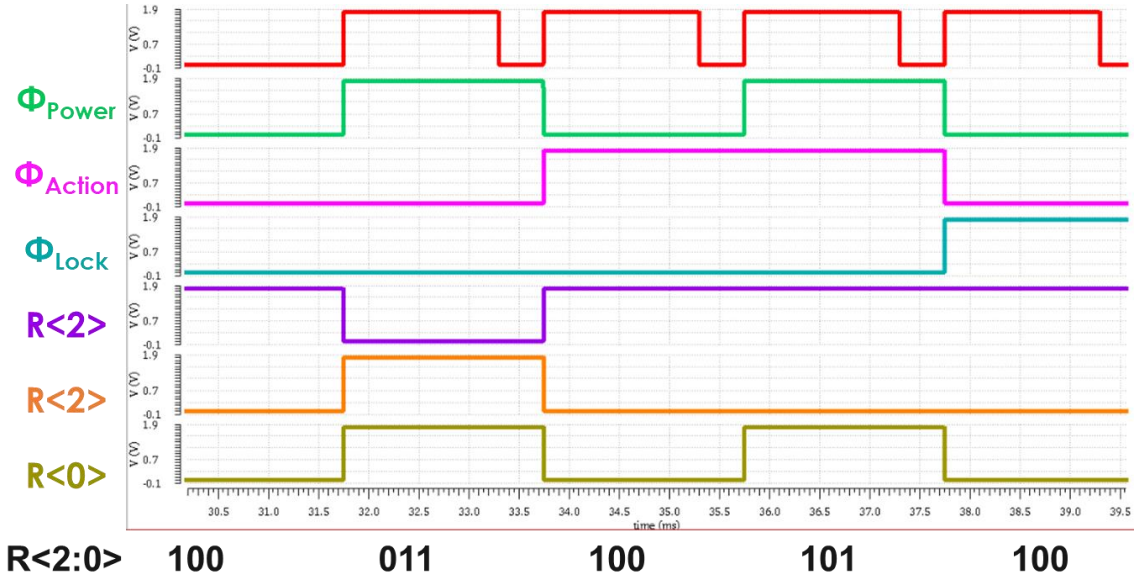

Figure 4.6 P&O decision circuits simulation results

Chapter 5: Conclusion

In this proposed work, a vibration energy harvesting system is presented. It adopts a rectifier along with dual-input dual-output architecture called dual-path three-switches convert as the power stage. It achieves rectification of AC source, maximum power extraction from source, and regulation of load two stages versus the traditionally three-stages system.

The key contribution of this work is the new MPPT method proposed. This new method incorporates two commonly used MPPT methods into one. It adopts the advantages of two previously existing methods and improves some of the disadvantages. The new MPPT method achieves accurate MPP in an energy-efficient way with shorter convergence time.

The IC implementation of the proposed work uses TSMC 180nm technology. The post-layout simulation results demonstrate the system functionality as expected.

5.1 Future Work

Currently, the FOCV mode of the proposed MPPT method is running under a fixed frequency clock, and it samples a new open circuit voltage at every single cycle. Sampling open circuit voltage requires disconnecting the load from the source which interrupted the harvesting time. In addition, the circuit needs time to converge to the desired operating point after sampling, energy is wasted during the time of sampling and recovering. Utilizing the power measurement circuit from P&O mode, a new mechanism could be added at each rising edge of the FOCV clock determining whether to trigger sampling or not. Sampling open circuit voltage will only get triggered if power changed

is observed. When the system remains the same working condition, sampling will not get triggered, thus the system gets less interruption from sampling and harvests energy at its maximum power point continuously.

Furthermore, a system on a chip (SoC) [20] could be developed to incorporate lower on-resistance of power mosfets, inductor, resistive ladder, and timing capacitors. Since the system has an input voltage that is higher than 5 V, the power mosfet needs a breakdown voltage that is higher than the maximum of input voltage. The current technology chosen has a high on-resistance for mosfet with high voltage breakdown. If power mosfet using a different technology that has low on-resistance as well as high voltage breakdown can the incorporated with the control circuit using currently chosen technology on the same chip, it will greatly reduce the conduction loss causing by the power mosfet. Having those passive components on a chip could further reduce the parasitics, increase the accuracy of clock, thus improve the overall efficiency of the system.

References

[1] C.-N. Xu, M. Akiyama, K. Nonaka, and T. Watanabe, “Electrical power generation characteristics of PZT piezoelectric ceramics,” IEEE Trans. Ultrason., Ferroelect., Freq. Control, vol. 45, pp. 1065–1070, July 1998.

[2] N. S. Hudak and G. G. Amatucci, "Small-scale energy harvesting through thermoelectric, vibration, and radiofrequency power conversion," Journal of Applied Physics, vol. 103, pp. 101301-1, 2008.

[3] C. O. Mathuna, T. O'Donnell, R. V. Martinez-Catala, J. Rohan, and B. O'Flynn, "Energy scavenging for long-term deployable wireless sensor networks," Talanta, vol. 75, pp. 613-623, 2008.

[4] J. A. Paradiso and T. Starner, "Energy scavenging for mobile and wireless electronics," IEEE Pervasive Computing, vol. 4, pp. 18-27, 2005.

[5] P. Glynne-Jones, S. P. Beeby, and N. M. White, “Towards a piezoelectric vibration powered microgenerator,” IEE Proc.-Sci. Meas. Technol., vol. 148, no. 2, pp. 68–72, 2001.

[6] G. Poulin, E. Sarraute, and F. Costa, “Generation of electrical energy for portable devices: Comparative study of an electromagnetic and a piezoelectric system,” Sens. Actuators A, Phys., vol. 116, no. 3, pp. 461–471, 2004.

[7] F. Dell'Anna et al., "State-of-the-Art Power Management Circuits for Piezoelectric Energy Harvesters," in IEEE Circuits and Systems Magazine, vol. 18, no. 3, pp. 27-48, third quarter 2018.

[8] Marco Balato, Luigi Costanzo, Alessandro Lo Schiavo, Massimo Vielli, “Optimization of both Perturb & Observe and Open Circuit Voltage MPPT Techniques for Resonant Piezoelectric Vibration Harvesters feeding bridge rectifiers”

[9] N. Kong and D. S. Ha, "Low-Power Design of a Self-powered Piezoelectric Energy Harvesting System with Maximum Power Point Tracking," in IEEE Transactions on Power Electronics, vol. 27, no. 5, pp. 2298-2308, May 2012.

[10] A. Erturk and D. J. Inman, “An experimentally validated bimorph cantilever model for piezoelectric energy harvesting from base excitations,” Smart Mater. Struct., vol. 18, pp. 025009 (18 pp.), 2009.

[11] S. Bandyopadhyay and A. P. Chandrakasan, "Platform Architecture for Solar, Thermal, and Vibration Energy Combining with MPPT and Single Inductor," *IEEE Journal of Solid-State Circuits*, vol. 47, no. 9, pp. 2199-2215, 2012.

[12] Y. Wang, Y. Huang, P. Huang, H. Chen and T. Kuo, "A Single-Inductor Dual-Path Three-Switch Converter With Energy-Recycling Technique for Light Energy Harvesting," in IEEE Journal of Solid-State Circuits, vol. 51, no. 11, pp. 2716-2728, Nov. 2016.

[13] H. Shao, X. Li, C. Tsui and W. Ki, "A Novel Single-Inductor Dual-Input Dual-Output DC–DC Converter With PWM Control for Solar Energy Harvesting System," in IEEE Transactions on Very Large Scale Integration (VLSI) Systems, vol. 22, no. 8, pp. 1693-1704, Aug. 2014.

[14] N. Kawai, Y. Kushino and H. Koizumi, "MPPT controlled piezoelectric energy harvesting circuit using synchronized switch harvesting on inductor," IECON 2015 - 41st

Annual Conference of the IEEE Industrial Electronics Society, Yokohama, 2015, pp. 001121-001126.

[15] Y. Hu, I. Chen and T. Tsai, "A piezoelectric vibration energy harvesting system with improved power extraction capability," 2016 IEEE Asian Solid-State Circuits Conference (A-SSCC), Toyama, 2016, pp. 305-308.

[16] H. Shao, C. Tsui and W. Ki, "The Design of a Micro Power Management System for Applications Using Photovoltaic Cells With the Maximum Output Power Control," in IEEE Transactions on Very Large Scale Integration (VLSI) Systems, vol. 17, no. 8, pp. 1138-1142, Aug. 2009.

[17] J. Wang, J. Li and D. S. Ha, "Energy Harvesting Circuit for Indoor Light based on the FOCV and P&O Schemes with an Adaptive Fraction Approach," ISCAS 2020.

[18] P.R. Gray, P. Hurst, R.G. Meyer, and S. Lewis, “Analysis and Design of Analog Integrated Circuits Reference”, Wiley, 2001.

[19] B. Razavi, “Design of Analog CMOS Integrated Circuits”, Boston, MA: McGraw-Hill, 2001.

[20] Wei Hwang, "New trends in low power SoC design technologies," IEEE International [Systems-on-Chip] SOC Conference, 2003. Proceedings., Portland, OR, USA, 2003, pp. 422.